Intercomparison of Arctic Regional Climate Models: Modeling Clouds and Radiation for SHEBA in May 1998

JUN INOUE

Institute of Observational Research for Global Change, Japan Agency for Marine-Earth Science and Technology, Yokosuka, Japan

JIPING LIU

School of Earth and Atmospheric Sciences, Georgia Institute of Technology, Atlanta, Georgia

JAMES O. PINTO

Department of Aerospace Engineering, University of Colorado, Boulder, Colorado

JUDITH A. CURRY

School of Earth and Atmospheric Sciences, Georgia Institute of Technology, Atlanta, Georgia

(Manuscript received 14 July 2005, in final form 2 November 2005)

ABSTRACT

To improve simulations of the Arctic climate and to quantify climate model errors, four regional climate models [the Arctic Regional Climate System Model (ARCSYM), the Coupled Ocean–Atmosphere Mesoscale Prediction System (COAMPS), the High-Resolution Limited-Area Model (HIRHAM), and the Rossby Center Atmospheric Model (RCA)] have simulated the annual Surface Heat Budget of the Arctic Ocean (SHEBA) under the Arctic Regional Climate Model Intercomparison Project (ARCMIP). The same lateral boundary and ocean surface boundary conditions (i.e., ice concentration and surface temperature) drive all of the models. This study evaluated modeled surface heat fluxes and cloud fields during May 1998, a month that included the onset of the surface icemelt. In general, observations agreed with simulated surface pressure and near-surface air properties. Simulation errors due to surface fluxes and cloud effects biased the net simulated surface heat flux, which in turn affected the timing of the simulated icemelt. Modeled cloud geometry and precipitation suggest that the RCA model produced the most accurate cloud scheme, followed by the HIRHAM model. Evaluation of a relationship between cloud water paths and radiation showed that a radiative transfer scheme in ARCSYM was closely matched with the observation when liquid clouds were dominant. Clouds and radiation are of course closely linked, and an additional comparison of the radiative transfer codes for ARCSYM and COAMPS was performed for clear-sky conditions, thereby excluding cloud effects. Overall, the schemes for radiative transfer in ARCSYM and for cloud microphysics in RCA potentially have some advantages for modeling the springtime Arctic.

1. Introduction

The Arctic Climate Impact Assessment (ACIA 2005) highlighted the Arctic as particularly important and vulnerable to global climate change. Simulated Arctic climates in global climate models vary widely as shown by the Atmospheric Model Intercomparison Project (AMIP) and the Coupled Model Intercomparison Project (CMIP) (e.g., Walsh et al. 2002). Despite the climatic significance of the Arctic, many physical processes that occur in the Arctic remain poorly understood (for a review, see Curry et al. 1996). It is therefore unsurprising that simulated Arctic climates vary widely, depending on the climate model and physical parameterizations used.

High-resolution regional climate models (RCMs) of the Arctic have the advantage over global models that neither vertical nor horizontal model resolution limit

Corresponding author address: Jun Inoue, Institute of Observational Research for Global Change (IORGC), Japan Agency for Marine-Earth Science and Technology (JAMSTEC), 2-15 Natsushima-cho, Yokosuka 237-0061, Japan.
E-mail: jun.inoue@jamstec.go.jp

the treatment of orography or physical processes (e.g., Rinke et al. 2000). Furthermore, parameterizations of physical processes unique to polar regions can be tested and implemented in RCMs to assess their interactions with the regional climate system. Arctic RCMs that are driven by analyzed lateral boundary conditions have the additional advantage of reduced impacts of potential errors introduced by same boundary conditions. RCMs can be used to elucidate the source of problems in global model simulations of the Arctic climate. In addition, RCMs are now run routinely for many situations and applications in the Arctic, including integrated assessment and policy studies (e.g., Lynch et al. 2004). In the context of such applications, error and uncertainty estimates are needed for RCM simulations of the Arctic climate.

The Arctic Regional Climate Model Intercomparison Project (ARCMIP) was developed (Curry and Lynch 2002) to improve climate modeling of the Arctic. ARCMIP is an international project organized under the auspices of the World Climate Research Program, Global Energy and Water Cycle Experiment (GEWEX) Cloud System Studies Working Group on Polar Clouds, and the Arctic Climate System Studies (ACSYS) Numerical Experimentation Group (NEG). The first ARCMIP experiment occurred between September 1997 and October 1998. Intensive observations from 1997 to 1998 under the auspices of the Surface Heat Budget of the Arctic Ocean (SHEBA) program (Uttal et al. 2002), the First International Satellite Cloud Climatology Project (ISCCP) Regional Experiment (FIRE) Arctic Clouds Experiment (Curry et al. 2000), and the Atmospheric Radiation Measurement (ARM) Program (Stamnes et al. 1999) have provided an unprecedented amount of data from the Arctic for model evaluation. Rinke et al. (2006) evaluated atmospheric dynamics of ARCMIP simulations, and Tjernström et al. (2005) evaluated the atmospheric boundary layer in ARCMIP simulations. This paper focuses on the surface heat balance and clouds in May 1998, a month that included the onset of surface snowmelt.

2. Overview of models and experimental design

Eight regional models simulated data for the first ARCMIP experiment (for model details, see Rinke et al. 2006; Tjernström et al. 2005). Four of these models were selected for the present study based on the completeness of archived data variables required:

- the Arctic Regional Climate System Model (ARCSYM: Lynch et al. 1995),
- the Coupled Ocean–Atmosphere Mesoscale Prediction System (COAMPS : Hodur 1997),

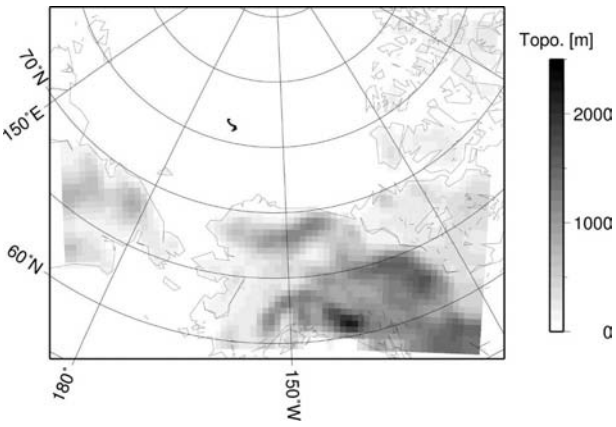

FIG. 1. Topography in the ARCMIP models. The black line denotes the SHEBA ice-drift track in May 1998.

- the High-Resolution Limited-Area Model (HIRLAM) with physics from ECHAM4, a GCM based on European Centre for Medium-Range Weather Forecasts (ECMWF) models modified and extended in Hamburg (HIRHAM4: Christensen et al. 1996), and
- the Rossby Center Atmospheric Model (RCA: Jones et al. 2004).

Figure 1 shows the simulation domain, which covers the western Arctic and includes the SHEBA drift trajectory. The domain also includes the ARM Barrow site and a few land-based sounding stations (e.g., Barrow and Fairbanks, Alaska). The model simulations were for the atmosphere only with specified ocean surface boundary conditions (ice concentration and surface temperature). The horizontal resolution of 50 km was roughly the same in all models, but the grid spacing could not be exactly the same, as the models used different grids and projections. The vertical resolution differed between models, as detailed by Tjernström et al. (2005) and Rinke et al. (2006). Initial and lateral model conditions were supplied by ECMWF analyses. The lower boundary conditions for sea ice concentration and surface temperature were provided by SSM/I satellite data (Comiso 2002) and the Advanced Very High Resolution Radiometer (AVHRR) satellite data (Key 2001), respectively. Each model run yielded gridded values over the western Arctic domain at 3-h intervals. Model output included three-dimensional fields of temperature, wind, humidity, height, and cloud properties at 12 different pressure levels and two-dimensional fields of radiation components, vertically integrated cloud properties, surface flux components, and precipitation.

Key to this study was the comparison of simulated output with SHEBA/ARM/FIRE observations. These

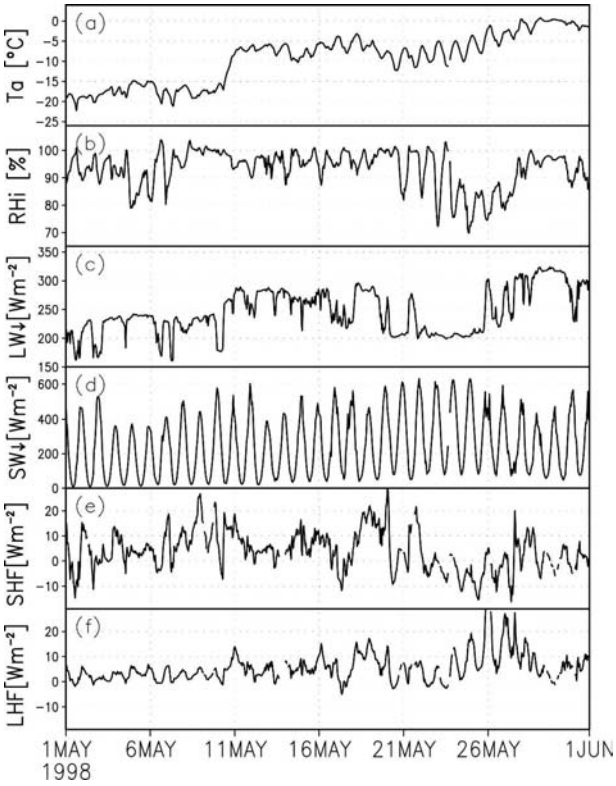

FIG. 2. Time series of meteorological parameters during May 1998 observed at the SHEBA tower: (a) 10-m air temperature, (b) 10-m relative humidity for ice, (c) downwelling longwave radiation flux, (d) downwelling shortwave radiation flux, (e) sensible heat flux, and (f) latent heat flux.

observations were summarized by Curry et al. (2000) and Uttal et al. (2002). Specifically, all model results were compared with measurements from the SHEBA Atmospheric Surface Flux Group (ASFG) instrument tower (Persson et al. 2002) and from radiosondes at the SHEBA site. Cloud radar images at the SHEBA site were also used (Shupe et al. 2001; Intrieri et al. 2002).

Analyses in this study focused on May 1998. This period was chosen because of the rapid increase in observed net surface heat flux and the complexity of boundary layer mixed phase clouds. In addition, the end of May coincided with the onset of surface melt. The SHEBA camp during May 1998 was located on pack ice in the Chukchi Sea near 76°N, 165°–167°W. Several cyclones passed over this region during May, reducing significantly the surface pressure (not shown) and influencing the temperature. For example, the air temperature increased 10 K from 11 to 13 May (Fig. 2a) as the first cyclone passed. Relatively high values of downward longwave (LWD) radiation and high values of surface relative humidity were consistent with the presence of clouds associated with cyclonic events

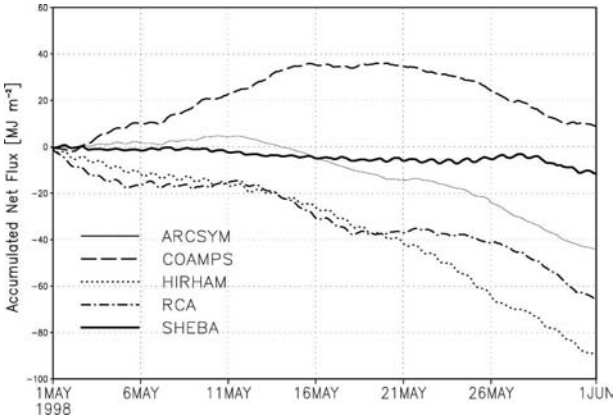

FIG. 3. Accumulated net heat flux (sum of radiation and turbulent heat fluxes) for each model in May 1998 (positive upward): ARCSYM (solid line); COAMPS (dashed line); HIRHAM (dotted line); RCA (dot–dashed line); SHEBA (thick line). Note that, in the accumulations, each 3-hourly value was considered representative for the entire corresponding 3-h period.

(Figs. 2b,c). Clear-sky conditions observed from 22 to 25 May were associated with high surface pressure and reduced LWD radiation. Sensible and latent heat fluxes varied between -10 and 30 W m^{-2} (Figs. 2e,f). The surface albedo decreased from 0.9 at the beginning of the month to 0.8 at the end of the month, indicating the onset of melting (not shown).

3. Evaluation

a. Surface fluxes

Figure 3 shows the accumulated net heat flux (sum of radiative and turbulent heat fluxes) to demonstrate how model surface flux errors propagated through the onset of surface snowmelt and icemelt. Observations showed that the melt season began on 29 May at the SHEBA site (Persson et al. 2002). Here, we defined that melting starts in each model when each modeled flux reaches the observed amount on 29 May 1998. HIRHAM and RCA predicted snowmelt onset at the beginning of May. In contrast, COAMPS estimated onset at the beginning of June. ARCSYM results agreed fairly well with observations.

Table 1 shows monthly mean error statistics, relative to the SHEBA observations, for simulated surface mean parameters (surface temperature, 2-m air temperature, air–sea temperature difference, 10-m water vapor mixing ratio, 10-m wind speed, and friction velocity) and turbulent heat fluxes. Comparisons were based on output from each model at the grid cell closest to the SHEBA track. Surface temperatures had a 2°C cold bias that arose from a local bias in the specified

TABLE 1. Monthly mean error statistics for surface temperature (T_s in °C), 2-m temperature (T_2 in °C), air–sea temperature difference (ΔT in °C), 10-m water vapor mixing ratio (Q_v in g kg^{-1}), 10-m wind speed (W in m s^{-1}), friction velocity (u_* in m s^{-1}), sensible and latent heat fluxes (SHF and LHF, respectively, positive upward), and net turbulent heat flux (Q_{turb} in W m^{-2}) for each model result. Bias indicates the mean error (model minus observation), and R is the correlation coefficient between the modeled result and the observation.

Model	T_s	T_2	ΔT	Q_v	W	u_*	SHF	LHF	Q_{turb}
Bias									
ARCSYM	−1.8	0.65	−2.3	0.20	3.0	−0.13	−4.2	−0.1	−4.3
COAMPS	−2.1	−1.5	−0.61	−0.19	3.0	−0.14	−3.5	−2.7	−6.2
HIRHAM	−2.0	−1.6	−0.48	−0.35	2.2	−0.12	−6.0	−1.2	−7.2
RCA	−2.3	−1.7	−0.68	−0.26	1.4	−0.12	−6.6	2.4	−4.3
R									
ARCSYM	0.87	0.93	0.33	0.87	0.61	0.56	0.31	0.20	0.35
COAMPS	0.87	0.90	0.34	0.85	0.57	0.60	0.37	0.26	0.38
HIRHAM	0.86	0.89	0.23	0.85	0.50	0.66	0.27	0.26	0.32
RCA	0.87	0.89	0.26	0.91	0.64	0.77	0.40	0.49	0.39

surface temperature field (see Tjernström et al. 2005). The surface air temperature and mixing ratio showed negative biases in COAMPS, HIRHAM, and RCA, generally corresponding to the surface temperature bias. In contrast, surface air temperatures and the mixing ratio had slightly positive biases in ARCSYM.

Although all four models showed comparable bias errors in friction velocity, the wind speed bias was smaller in HIRHAM and RCA. The surface layer parameterization used in COAMPS, HIRHAM, and RCA was from Louis (1979) and based on the Monin–Obukhov similarity theory for the surface layer. Parameterization in ARCSYM followed Bitz's ice model (Bitz and Lipscomb 1999; Bitz et al. 2001) including the effect of conductive heat flux from the ice/snow interior. Because turbulent fluxes in the Arctic are generally small in magnitude, bias errors were nearly comparable to measurement accuracy [i.e., the random errors for sensible heat (±4.1 W m^{-2}) and latent heat (±50% ≈ ±2.8 W m^{-2}) fluxes at the tower (Persson et al. 2002)]. Modeled surface turbulent fluxes thus showed fairly low correlations with observations, and bias errors were of the same order as the fluxes themselves.

Table 2 shows monthly mean error statistics for radiative fluxes relative to the SHEBA observations. The largest bias error for downward shortwave (SWD) radiation, which was determined by cloud cover and surface albedo, occurred using ARCSYM (−54 W m^{-2}), followed by RCA (33 W m^{-2}). The bias errors for HIRHAM and COAMPS were very small, but the correlation coefficient in HIRHAM was relatively low. Small errors in net shortwave flux occurred using COAMPS. Due to the compensating effect of large errors in SWU and SWD radiation, the net shortwave radiation in ARCSYM seems small. Net shortwave flux from HIRHAM had a relatively large bias error because of bias error for SWU associated with the surface albedo parameterization. This feature was also found in Tjernström et al. (2005). The ice albedo in HIRHAM depends only on the ice-surface temperature, although

TABLE 2. As in Table 1 but for surface radiation fluxes (W m^{-2}): downward and upward shortwave fluxes ($SW_\downarrow$ and $SW_\uparrow$), net shortwave flux (SW_{net}: positive upward), downward and upward longwave fluxes ($LW_\downarrow$ and $LW_\uparrow$), net longwave flux (LW_{net}: positive upward), and total radiative flux (Q_{rad}: positive upward).

Model	$SW_\downarrow$	$SW_\uparrow$	SW_{net}	$LW_\downarrow$	$LW_\uparrow$	LW_{net}	Q_{rad}
Bias							
ARCSYM	−53.9	−48.6	5.7	7.5	−4.8	−12.3	−6.5
COAMPS	−1.0	2.7	3.7	−16.4	−5.4	11.0	14.7
HIRHAM	−3.0	−40.8	−37.8	−21.7	−5.0	16.8	−21.1
RCA	33.0	20.9	−12.2	−2.0	−4.8	−2.7	−14.9
R							
ARCSYM	0.80	0.80	0.71	0.57	0.85	0.14	0.57
COAMPS	0.91	0.92	0.80	0.27	0.85	−0.29	0.41
HIRHAM	0.71	0.73	0.58	0.62	0.84	0.25	0.53
RCA	0.91	0.93	0.80	0.57	0.84	0.39	0.65

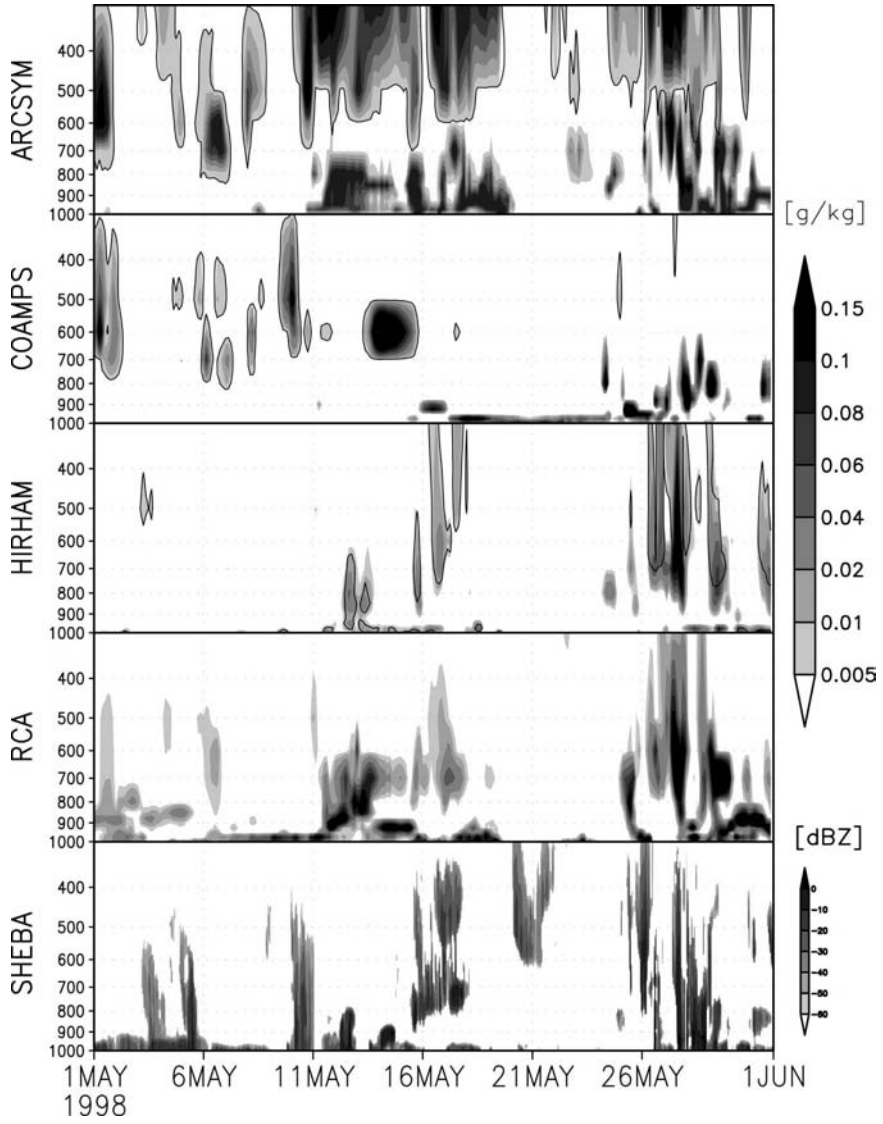

FIG. 4. Time–height cross sections of the sum of simulated water and ice mixing ratios (shaded regions, ordinate unit: hPa). The contour indicates ice mixing ratio exceeding 0.005 g kg^{-1}. Only the sum of water and ice mixing ratios is available in RCA. (bottom) The cloud radar reflectivity (dBZ) at the SHEBA site.

the more sophisticated parameterizations, that is, snow depth and ice thickness in ARCSYM, give more realistic basinwide albedo variability (Liu et al. 2006). Errors in the modeled upward longwave (LWU) radiation were consistent with errors in surface temperature (Table 1). Biases in LWD radiation were large for HIRHAM and COAMPS.

b. Clouds and precipitation

Model errors most obviously arose from the properties of simulated clouds and simulated atmospheric temperature and humidity profiles. Figure 4 shows time–height cross sections of the liquid water equivalent mixing ratio (shaded) and ice mixing ratio exceeding 0.005 g kg^{-1} (contour) for each model to assess simulated cloud properties in the ARCMIP models. Observed cloud radar reflectivity is also shown in the bottom panel. From the observation, we selected three main cloudy periods: (I) 1–10 May, (II) 11–19 May, and (III) 29–31 May 1998. Scatterplots of the simulated SWD and LWD radiation for each model compared to the observation are also shown in Figs. 5 and 6.

RCA cloud geometry agreed best with observations, although the simulated ice and liquid water contents were somewhat smaller than observed (as discussed in

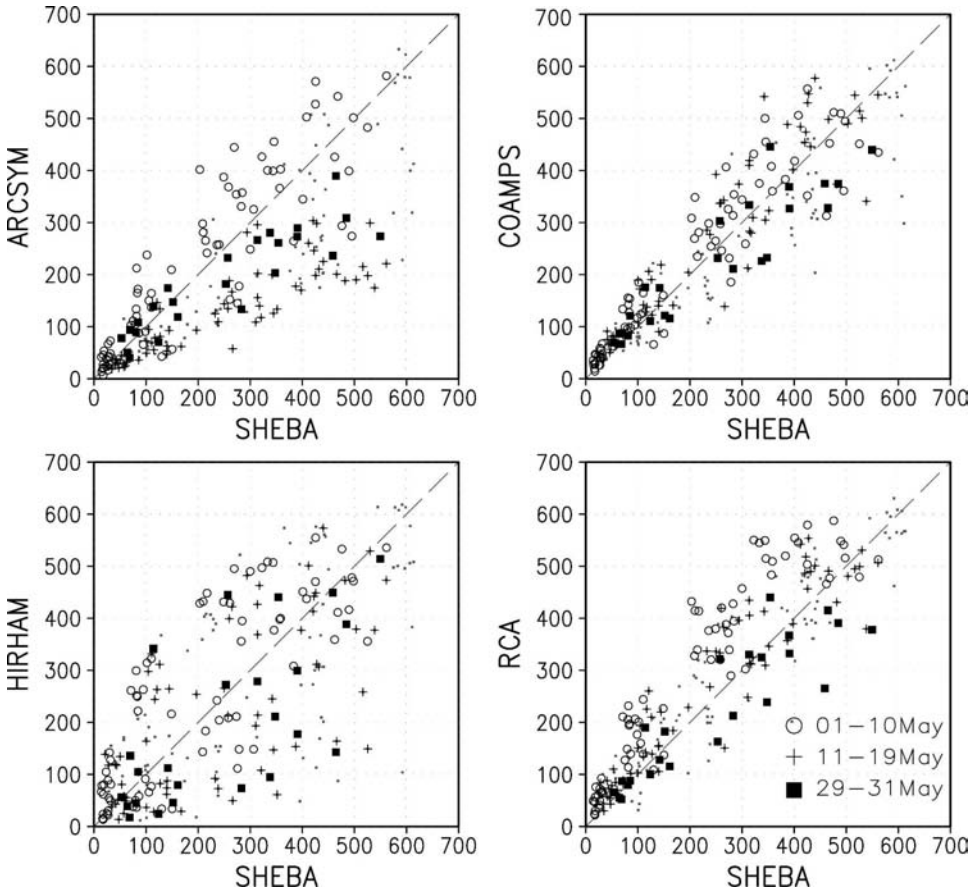

FIG. 5. Scatterplots of the modeled (vertical axis) against the observed (horizontal axis) downwelling shortwave radiation (W m^{-2}) during the three specific periods. Gray dots denote the one during the other period.

section 3c), resulting in large values of simulated SWD radiation, in particular during periods I and II (Fig. 5). The simulated cloud geometry by HIRHAM relatively matched with the observations, while the simulated cloud mixing ratio values were much lower in RCA and are missing within the first half of the month, which had ratios consistent with the large negative bias in the simulated LWD radiation during period I (Fig. 6). COAMPS cloud geometry deviated substantially from the observed clouds, especially for low clouds. COAMPS simulated low clouds when clear skies were observed on 22–25 May; COAMPS also did not show the low clouds that were observed during periods I and II. Errors in cloud simulations caused the lowest correlation coefficient for LWD radiation (Table 2 and Fig. 6). ARCSYM results showed the largest errors in simulated cloud geometry. ARCSYM predicted extensive ice clouds in the mid and upper troposphere. This overestimate of upper-level clouds was consistent with the large negative bias in SWD radiation except for period I (Fig. 5). The negative bias in LWD radiation in the presence of substantial overestimates of ice water content arose from the relatively cold temperature (high altitude) of the emitting clouds during period I (Fig. 6).

Variations and discrepancies in simulated cloud geometry may partially depend on vertical profiles of air temperature and humidity. Figure 7 shows time–height cross sections of temperature biases in May 1998 between the air temperature at the closest grid to the SHEBA site and the SHEBA soundings. All models showed a negative bias for air temperature above 900 hPa, in particular during the clear-sky condition (22–25 May). ARCSYM showed the largest error. The cloud-free area has a partially negative bias (e.g., during 5–11 May). The cold bias at low altitudes for COAMPS, HIRHAM, and RCA in particular during periods II and III was consistent with the cold bias in surface temperature. Figure 8 shows time–height cross sections of relative humidity (contours indicate relative humidity with respect to ice with saturation above 100%). Relative humidity simulated by HIRHAM and

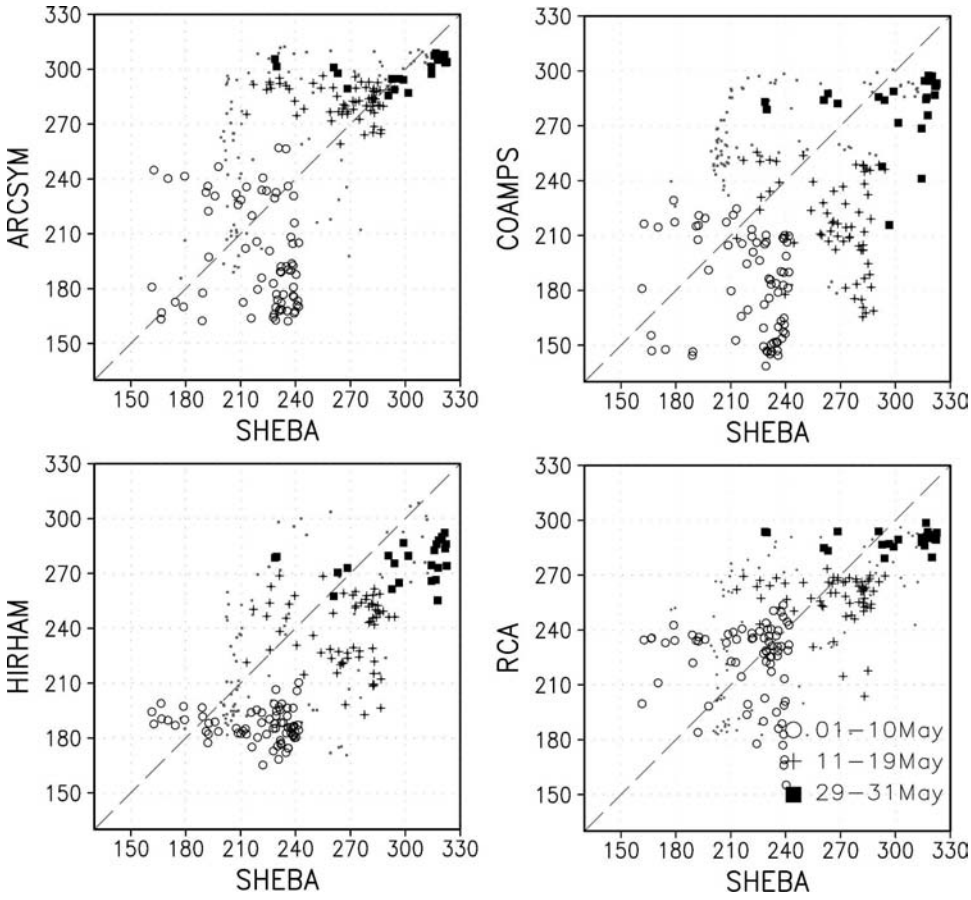

FIG. 6. As in Fig. 5 but for downwelling longwave radiation (W m^{-2}).

RCA generally agreed with observations. Figure 4, however, shows that the cloud fields (i.e., mixing ratio) differed significantly between the two models, especially the low-level clouds.

The cloud scheme in HIRHAM was based on that by Sundqvist (1978), who suggested that condensation processes on a model grid can be treated as subgrid-scale processes so that cloud formation actually initiates before the grid-resolved humidity reaches saturation (when a critical relative humidity is reached) and, thus, before a cloud cover fraction is defined. Precipitation produced by the model could evaporate or sublimate below the cloud base. The cloud scheme in RCA was based on Rasch and Kristjánsson (1998), which is a simplified treatment of the ice phase compared to the Sundqvist scheme. Cloud ice is diagnosed from grid-point temperature with a probability distribution function and then used as a parameter in the microphysical functions where it is needed. This scheme makes a much closer connection between the meteorological processes that determine condensate formation and condensate amount. They also noted that ice and liquid water burdens were about 30% higher than in the standard model configuration under the Sundqvist scheme, providing the largest significant improvements in polar regions. This characteristic was present in comparisons of vertical cloud distributions from HIRHAM and RCA (Fig. 4). The RCA cloud scheme therefore has some advantages in terms of cloud microphysics performance.

Analysis of the simulated precipitation also demonstrates the difference of both schemes. The precipitation in the middle of May is significantly important for change in the surface albedo because some models parameterize the albedo using snowfall as mentioned before. Figure 9 shows liquid water equivalent accumulated precipitation from the simulations and from the rain gauge at the SHEBA site. Observations showed significant precipitation on 11–13 and 29–30 May. Both events were successfully reproduced by COAMPS and RCA; however, the total accumulated precipitation in this month was almost 50% greater than observed primarily because precipitation in the latter event was overestimated. Neither ARCSYM nor HIRHAM simu-

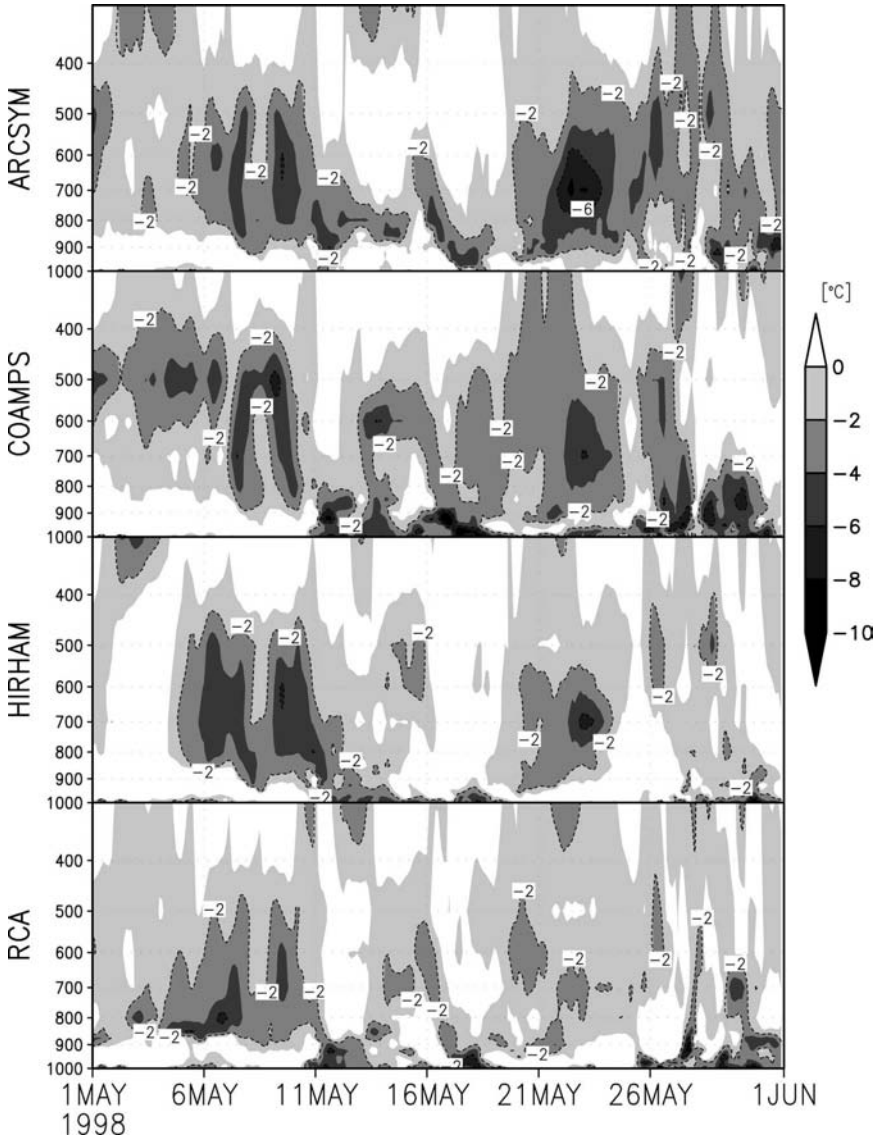

FIG. 7. Time–height cross sections of the temperature bias in May over the SHEBA site between modeled and observed results.

lated any significant precipitation until nearly the end of the month.

c. Radiative transfer

Clouds have a complex effect on surface radiation fluxes that depend on particle phase, size, shape, concentration, cloud-base height, geometric cloud depth, and cloud fraction. If the cloud optical depth is too large, then the simulated SWD radiation will be too small and the LWD radiation will be too large. Because there is little compensation in the signs and magnitudes of the longwave and shortwave fluxes, it is likely that other factors, such as surface albedo, cloud-base temperature, and the radiative transfer models, contribute to simulation errors.

Modeled and observed relationships between cloud microphysics [expressed in terms of liquid water path (LWP) and ice water path (IWP)] and LWD radiation are shown in Fig. 10. In the observation, LWD radiation increases with LWP until LWP = 0.1 kg m^{-2} and increasing LWP has no further impact on LWD radiation. There are three curves in the observations around 240, 280, and 320 W m^{-2}, corresponding the following periods: (I) 1–10 May, (II) 11–19 May, and (III) 29–31 May 1998. This scatter might be due to the air temperature (Fig. 2a). On the contrary, these relationships are not always satisfied in each model. In period I, the

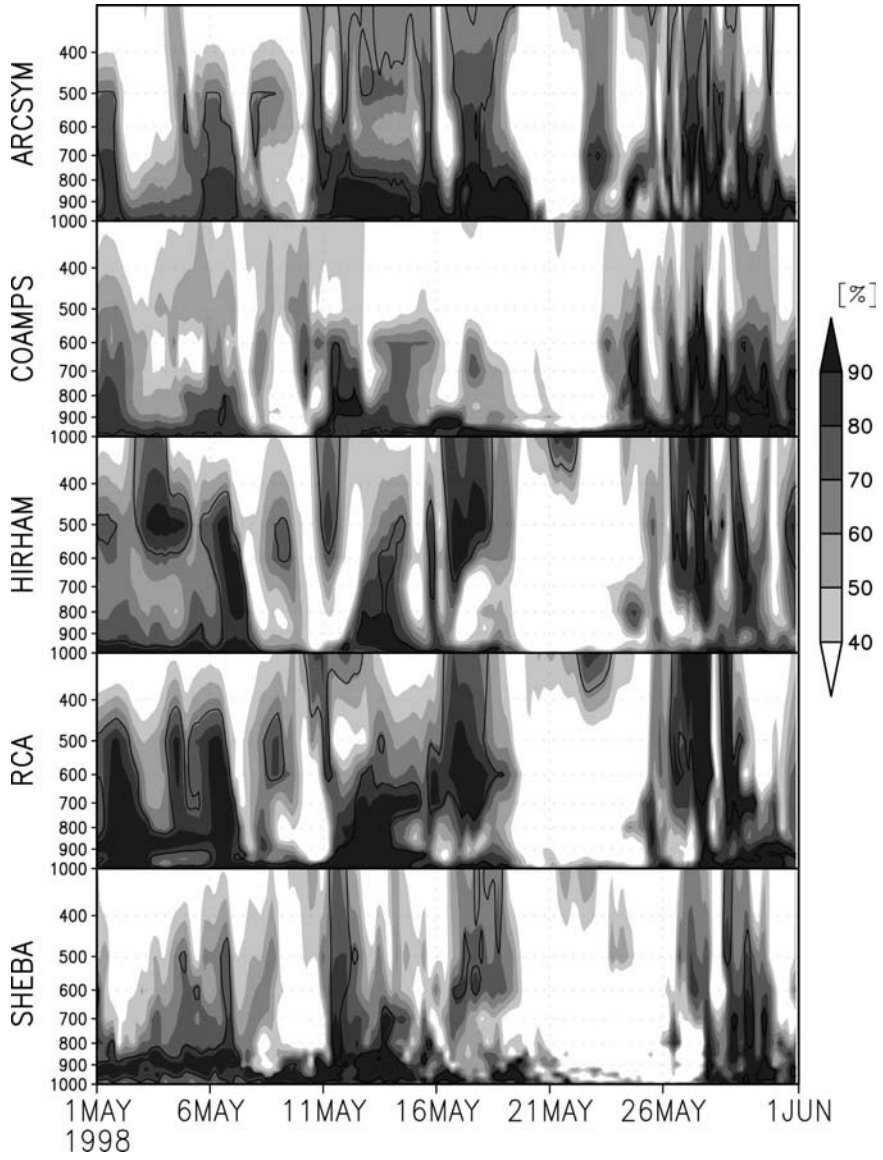

FIG. 8. Time–height cross sections of relative humidity (ordinate unit: hPa). The contour indicates where relative humidity with respect to ice saturation exceeded 100%.

amount of LWD radiation for ARCSYM and COAMPS is relatively close to the observation although both model dominate ice clouds (Fig. 4). HIRHAM is hard to compare due to small amount of LWP and IWP in the period. RCA shows a small amount of LWD radiation between 0.02 and 0.04 kg m^{-2}. Variation in period II among the models is the largest; ARCSYM is the best, followed by RCA, while COAMPS is 80 W m^{-2} smaller than the observed one, suggesting that ice clouds are dominant, that is, errors of cloud phase and/or cloud-base height). In general, ice particles are typically larger than liquid droplets but have a smaller relative mass density and occur in smaller concentrations; consequently liquid-containing cloud scenes are important for LWD radiation (Shupe and Intrieri 2004). The curve for period III is the best case for comparison of radiative transfer because all models have liquid water clouds in the lower boundary layer. The amount of LWD radiation is scattered from the observation within 10–40 W m^{-2}. ARCSYM simulated LWD radiation well, while the other models have a clear negative bias about 40 W m^{-2}. Overall, ARCSYM reproduced well the simulated relationship between LWD radiation and cloud water paths under cloudy-sky conditions.

Under clear-sky condition, the radiative transfer codes in ARCSYM and COAMPS could not function

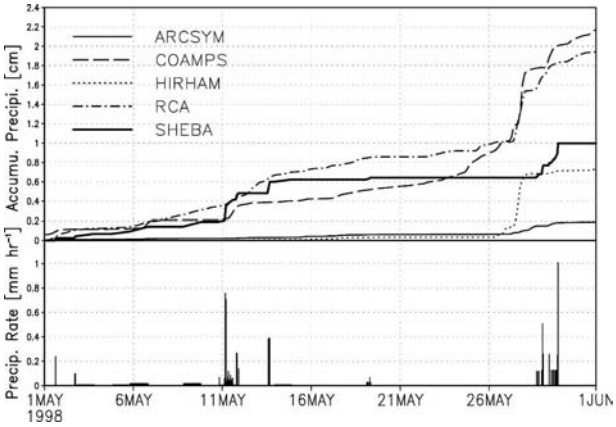

FIG. 9. Time series of the liquid water equivalent accumulated from modeled results (ARCSYM: solid line; COAMPS: dashed line; HIRHAM: dotted line; RCA: dot–dashed line) and from the rain gauge at the SHEBA site (thick line). (bottom) The observed precipitation rate.

properly because of cloud field misrepresentations (Fig. 4). Thus, an additional comparison between the radiative transfer models of ARCSYM and COAMPS is warranted. The Arctic Radiation Model Intercomparison Project (more information available online at http://www.rap.ucar.edu/projects/GCSS/WG5/rad_intcmp/) was conducted under the auspices of the World Climate Research Program (WCRP) GEWEX Cloud System Studies Working Group on Polar Clouds. A special case was selected to evaluate stand-alone radiative transfer codes in ARCSYM [Briegleb (1992) for shortwave radiation, and Mlawer et al. (1997) for longwave radiation] and COAMPS (Harshvardhan et al. 1987) (HIRHAM and RCA radiation codes were not available for this project). Cloud effects on radiative fluxes were excluded by selecting a clear-day case (24 May 1998) that met several criteria: first, the atmosphere was reasonably stationary and homogeneous; second, aircraft measurements of in situ atmospheric characteristics were available for the same time period; and finally, extensive surface-based radiation data were present. Input files that contained information on the vertical structure of the atmosphere were generated to test the radiative transfer codes. These data were gridded in the vertical using the nearest data values obtained from the Geoscience Laser Altimeter System (GLAS) radiosonde for 2325 UTC on 24 May 1998. Aerosol profiles were determined from aerosol measurements taken by the NCAR C-130 aircraft below 6 km and from a combination of climatology and total-column optical-depth data from the Multifilter Rotating Shadowband Radiometer (MFRSR) above 6 km.

The bias of LWD radiation in ARCSYM and

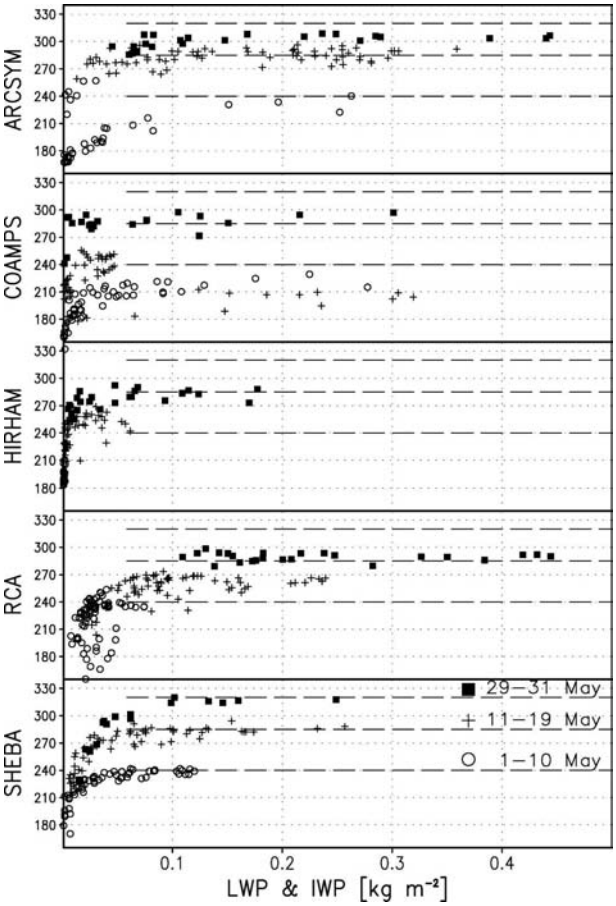

FIG. 10. Relationship between total water path [sum of LWP and IWP (g m^{-2})] and downwelling longwave radiation flux (W m^{-2}) for each model and observation.

COAMPS was −4 and −18 W m^{-2}, respectively, under clear-sky conditions. Even if the effect of clouds on LWD radiation was excluded, COAMPS code produced an error larger than the monthly mean (−16 W m^{-2}: Table 2). In contrast, ARCSYM results closely matched observations. Pinto et al. (1997) also compared several radiative transfer models for clear-sky conditions during Arctic spring as part of the 1992 Arctic Leads Experiment (LEADEX). The Rapid Radiative Transfer Model (RRTM) (Mlawer et al. 1997) that was used in ARCSYM produced values that most closely matched the observed LWD radiation. In contrast, schemes in COAMPS (Harshvardhan et al. 1987) and HIRHAM (Morcrette 1991) significantly underestimated the flux, in agreement with the present results. The bias in ARCSYM and COAMPS for SWD radiation under clear-sky conditions was −9 and −20 W m^{-2}, respectively. The monthly mean biases were −54 W m^{-2} (ARCSYM) and −1 W m^{-2} (COAMPS); thus, the shortwave radiative transfer code in ARCSYM has clear advantages.

4. Summary

Four ARCMIP models were compared with each other and with SHEBA observations for May 1998. Each model showed significant and different biases for surface fluxes. ARCSYM had the smallest net radiation bias; however, a compensating error was found in the shortwave flux, resulting from errors in the modeled cloud fields. This error also influenced LWD radiation. COAMPS most accurately simulated shortwave flux, but LWD radiation errors directly affected the net radiative flux and delayed the icemelt. HIRHAM showed the largest bias for net shortwave radiation due to underestimates of the ice surface albedo. In addition, underestimates of clouds caused the largest negative bias for LWD radiation. These two factors caused the largest error in net radiative flux. RCA also had a compensating error in the shortwave flux similar to that in ARCSYM. No model stood out as the best in terms of flux components. Difficulties arose mainly from errors in the cloud fields.

The investigations of cloud properties focused on the vertical cloud distribution and precipitation. Vertical cloud distribution was most poorly simulated by ARCSYM, particularly the amount of upper ice clouds. Low-level clouds persisted during clear-sky conditions in COAMPS, forcing a serious error in LWD radiation. HIRHAM underestimated cloud formation resulting in the largest bias in LWD radiation. RCA yielded the best simulation. Accumulated precipitation in the ARCMIP models could be classified into two groups: too much precipitation (COAMPS and RCA) and too little precipitation (ARCSYM and HIRHAM). Overall, the cloud scheme in RCA best reproduced the simulated cloud geometry and the precipitation associated with two important synoptic events.

Radiative transfer under cloudy-sky condition was evaluated focusing on a relationship between LWP (IWP) and LWD radiation during three different cloudy periods. Basically, the absence of liquid cloud made an adequate estimate of LWD radiation difficult in each model. In periods when liquid clouds dominated, ARCSYM agreed with the observations. For clear-sky conditions, an additional comparison of radiative transfer codes in ARCSYM and COAMPS, which could not be evaluated because of large cloud field errors, was conducted. Even though cloud effects were excluded, problems remained in the shortwave and longwave radiative schemes of COAMPS. In contrast, errors in ARCSYM were significantly reduced, suggesting that the radiative transfer codes in ARCSYM might work properly if clouds were correctly simulated.

In summary, this model intercomparison study showed that the ARCSYM radiative scheme and the RCA cloud scheme have some advantages for springtime Arctic simulations. Annual mean biases for surface fluxes computed in previous studies (e.g., Rinke et al. 2006) were smaller than biases in this study. This suggests the presence of potentially compensating errors in the annual statistics, and that the transitional season for melting remains one of the most challenging for Arctic climate simulation.

Acknowledgments. We acknowledge the invaluable work by the ARCMIP team in setting up the ARCMIP program, including the generation of the boundary and forcing fields for this experiment. In particular, we are grateful to A. H. Lynch and J. Key. We thank the climate modeling group of ARCSYM (J. Cassano), COAMPS (M. Tjernström and M. Zăgar), HIRHAM (A. Rinke and K. Dethloff), and RCA (K. Wyser and C. G. Jones). We also thank the SHEBA atmospheric surface flux group, GLAS sounding group, and NOAA/ETL cloud radar group for access to their observational data. We acknowledge two anonymous reviewers for their valuable comments. This work was supported by NASA NRA-02-OES-06 and the DOE ARM Program.

REFERENCES

ACIA, 2005: *Impact of a Warming Climate.* Cambridge University Press, 139 pp.

Bitz, C. M., and W. H. Lipscomb, 1999: An energy-conserving thermodynamic model of sea ice. *J. Geophys. Res.,* **104,** 15 669–15 677.

——, M. M. Holland, A. J. Weaver, and M. Eby, 2001: Simulating the ice-thickness distribution in a coupled climate model. *J. Geophys. Res.,* **106,** 2441–2463.

Briegleb, B. P., 1992: Delta-Eddington approximation for solar radiation in the NCAR Community Climate Model. *J. Geophys. Res.,* **97,** 7603–7612.

Christensen, J. H., O. B. Christensen, P. Lopez, E. van Meijgaard, and M. Botzet, 1996: The HIRHAM4 regional atmospheric climate model. DMI Science Rep. 96-4, Danish Meteorological Institute, Copenhagen, Denmark, 51 pp.

Comiso, J., 2002: *Bootstrap Sea Ice Concentrations for NIMBUS-7 SMMR and DMSP SSM/I.* National Snow and Ice Data Center, Boulder, CO, CD-ROM.

Curry, J. A., and A. H. Lynch, 2002: Comparing Arctic regional climate models. *Eos, Trans. Amer. Geophys. Union,* **83,** 87.

——, W. B. Rossow, D. Randall, and J. L. Schramm, 1996: Overview of Arctic cloud and radiation characteristics. *J. Climate,* **9,** 1731–1764.

——, and Coauthors, 2000: FIRE Arctic Clouds Experiment. *Bull. Amer. Meteor. Soc.,* **81,** 5–29.

Harshvardhan, R. Davies, D. A. Randall, and T. G. Corsetti, 1987: A fast radiation parameterization for atmospheric circulation models. *J. Geophys. Res.,* **92,** 1009–1016.

Hodur, R. M., 1997: The Naval Research Laboratory's Coupled Ocean/Atmosphere Mesoscale Prediction System (COAMPS). *Mon. Wea. Rev.,* **125,** 1414–1430.

Intrieri, J. M., M. D. Shupe, T. Uttal, and B. J. McCarty, 2002: An annual cycle of Arctic cloud characteristics observed by radar and lidar at SHEBA. *J. Geophys. Res.,* **107,** 8030, doi:10.1029/2000JC000432.

Jones, C. G., K. Wyser, A. Ullersting, and U. Willén, 2004: The Rossby Center regional atmospheric climate model. Part II: Application to the Arctic. *Ambio,* **33,** 211–220.

Key, J., 2001: The cloud and surface parameter retrieval (CASPR) system for polar AVHRR data user's guide. Space Science and Engineering Center, University of Wisconsin—Madison, Madison, WI, 62 pp.

Liu, J., Z. Zhang, J. Inoue, and R. M. Horton, 2006: Evaluation of snow/ice albedo parameterizations and their impacts on sea ice simulations. *Int. J. Climatol.,* in press.

Louis, J. F., 1979: A parametric model of vertical eddy fluxes in the atmosphere. *Bound.-Layer Meteor.,* **17,** 187–202.

Lynch, A. H., W. L. Chapman, J. E. Walsh, and G. Weller, 1995: Development of a regional climate model of the western Arctic. *J. Climate,* **8,** 1555–1570.

——, J. A. Curry, R. D. Brunner, and J. A. Maslanik, 2004: Toward an integrated assessment of the impacts of extreme wind events on Barrow, Alaska. *Bull. Amer. Meteor. Soc.,* **85,** 209–221.

Mlawer, E. J., S. J. Taubman, P. D. Brown, M. J. Iacono, and S. A. Clough, 1997: Radiative transfer for inhomogeneous atmospheres: RRTM, a validated correlated k model for the longwave. *J. Geophys. Res.,* **102,** 16 663–16 682.

Morcrette, J.-J., 1991: Radiation and cloud radiative properties in the European Centre for Medium-Range Forecasts forecasting system. *J. Geophys. Res.,* **96,** 9121–9132.

Persson, P. O. G., C. W. Fairall, E. L Andreas, P. S. Guest, and D. K. Perovich, 2002: Measurements near the Atmospheric Surface Flux Group Tower at SHEBA: Near-surface conditions and surface energy budget. *J. Geophys. Res.,* **107,** 8045, doi:10.1029/2000JC000705.

Pinto, J. O., J. A. Curry, and C. W. Fairall, 1997: Radiative characteristics of the Arctic atmosphere during spring as inferred from ground-based measurements. *J. Geophys. Res.,* **102,** 6941–6952.

Rasch, P. J., and J. E. Kristjánsson, 1998: A comparison of the CCM3 model climate using diagnosed and predicted condensate parameterizations. *J. Climate,* **11,** 1587–1614.

Rinke, A., A. H. Lynch, and K. Dethloff, 2000: Intercomparison of Arctic regional climate simulations: Case studies of January and June 1990. *J. Geophys. Res.,* **105,** 29 669–29 683.

——, and Coauthors, 2006: Evaluation of an ensemble of Arctic regional climate models: Spatiotemporal fields during the SHEBA year. *Climate Dyn.,* **26,** 459–472.

Shupe, M. D., and J. M. Intrieri, 2004: Cloud radiative forcing of the Arctic surface: The influence of clouds properties, surface albedo, and solar zenith angle. *J. Climate,* **17,** 616–628.

——, T. Uttal, S. Y. Matrosov, and A. S. Frisch, 2001: Cloud water contents and hydrometeor sizes during the FIRE Arctic Clouds Experiment. *J. Geophys. Res.,* **106,** 15 015–15 028.

Stamnes, K., R. G. Ellingson, J. A. Curry, J. E. Walsh, and B. D. Zak, 1999: Review of science issues, deployment strategy, and status for the ARM North Slope of Alaska–Adjacent Arctic Ocean Climate Research Site. *J. Climate,* **12,** 46–63.

Sundqvist, H., 1978: A parameterization scheme for nonconvective condensation including prediction of cloud water content. *Quart. J. Roy. Meteor. Soc.,* **104,** 677–690.

Tjernström, M., and Coauthors, 2005: Modelling the Arctic boundary layer: An evaluation of six ARCMIP regional-scale models with data from the SHEBA project. *Bound.-Layer Meteor.,* **117,** 337–381.

Uttal, T., and Coauthors, 2002: Surface Heat Budget of the Arctic Ocean. *Bull. Amer. Meteor. Soc.,* **83,** 255–275.

Walsh, J. E., V. M. Kattsov, W. L. Chapman, V. Govorkova, and T. Pavlova, 2002: Comparison of Arctic climate simulations by uncoupled and coupled global models. *J. Climate,* **15,** 1429–1446.